The Selection and performance of Diamond Radiators used in Coherent Bremsstrahlung Experiments

J. Kellie [a] P.J.M. Clive [a] G.L. Yang [a] C. Hall [e] C. Gordon [a]
C. McGeorge [a] D. Watts [a] J. W. Harris [b] J. Melone [a]
K. Livingston [a] P. Slaven [d] R.O. Owens [a] R. Vrcelj [c]

[a] *Dept. of Physics and Astronomy, University of Glasgow, Glasgow, Scotland*
[b] *Division of Earth Sciences, University of Glasgow, Glasgow, Scotland*
[c] *Dept. of Chemistry, University of Southampton, Southampton, England*
[d] *University of Strathclyde, Glasgow, Scotland*
[e] *Drukker International B.V., The Netherlands*

Abstract

The bremsstrahlung emitted as a result of scattering electrons in thin diamond crystals provides a useful source of high energy photons for use in photonuclear experiments. A primary electron beam is directed onto the diamond at an angle which produces coherent scattering known as coherent bremsstrahlung. This results in an enhancement of the photon spectrum which is linearly polarised. Techniques for selecting the most favourable diamonds have been investigated. These are optical crossed polaroid analysis, X-ray topography and rocking curve measurements. The diamonds are characterised with a view to determining their performance as radiators, and bremsstrahlung spectra from a diamond radiator used at the Mainz MAMI-B facility are presented.The changes caused by high energy electrons to the crystal properties of the diamond and to the resulting coherent bremsstrahlung spectra are discussed.

Key words: Bremsstrahlung; Diamonds; Coherent Bremsstrahlung; Photonuclear studies

1 Introduction

A well established method for creating a beam of high energy linearly polarised photons for use in photonuclear studies is coherent bremsstrahlung production

(1). The primary electron beam is scattered in a crystal whose regular lattice of atoms allows the recoil momentum to be taken up by the crystal as a whole, rather than by individual atoms. This occurs when the recoil momentum is equal to one of the crystal reciprocal lattice vectors, in a manner analogous to Bragg scattering.
In comparison to an incoherent bremsstrahlung spectrum from an amorphous radiator, a coherent bremsstrahlung spectrum has additional structure. Typical measured and calculated coherent and incoherent bremsstrahlung spectra are compared in figure 1. The black curves show the total measured photon energy spectra from nickel (top) and diamond (bottom). The red curves show theoretical fits to the data. Figure 2 shows the total photon spectrum from a diamond divided by its incoherent component, i.e. the relative intensity.
The main advantage of coherent bremsstrahlung is that the photons are linearly polarised. For example at selected photon energies, the degree of linear polarisation can exceed 80% if the photon beam is suitably collimated. Diamond is particularly suitable as a radiator due to its high Debye temperature, which means that since the amplitude of the thermal motion of the atoms in the lattice is small, the lattice structure is relatively unaffected by thermal effects. (2; 3).
Since diamond specimens always suffer from imperfections, one of the aims of the present study has been to find the extent to which they can be tolerated in coherent bremsstrahlung experiments. This can then be used as the basis for selecting suitable specimens. Ideally, the assessment technique should be simple and inexpensive but provide sufficient information to determine how well the diamond will perform as a radiator.
Diamonds are classified into four types, referred to as Ia, Ib, IIa and IIb (4). Type I have concentrations of nitrogen impurity varying from around 1 ppm. to greater than 10^3 ppm. The nitrogen in type Ia occurs in aggregated form, that is, the nitrogen atoms occur in the lattice in pairs, groups of four, or as part of other complexes formed with vacancies. In type Ib the nitrogen atoms are dispersed evenly through the volume of the diamond. Type II diamonds contain much less nitrogen than type I, in general less than 1 ppm. For natural diamonds, type II specimens are most probably the result of slow diamond growth. In the present paper both natural and synthetic industrial diamonds are assessed.

When an electron beam passes through a diamond radiator there is a spread in the direction of the electrons with respect to the crystal orientation due to three main causes; the divergence of the primary electron beam, multiple scattering of the electrons in the diamond and finally the variation in the crystal lattice arising from crystal defects. This angular variation degrades the coherent spectrum and it should be kept smaller than the bremsstrahlung characteristic opening angle,

$$\theta_{br} = \frac{mc^2}{E_0}$$

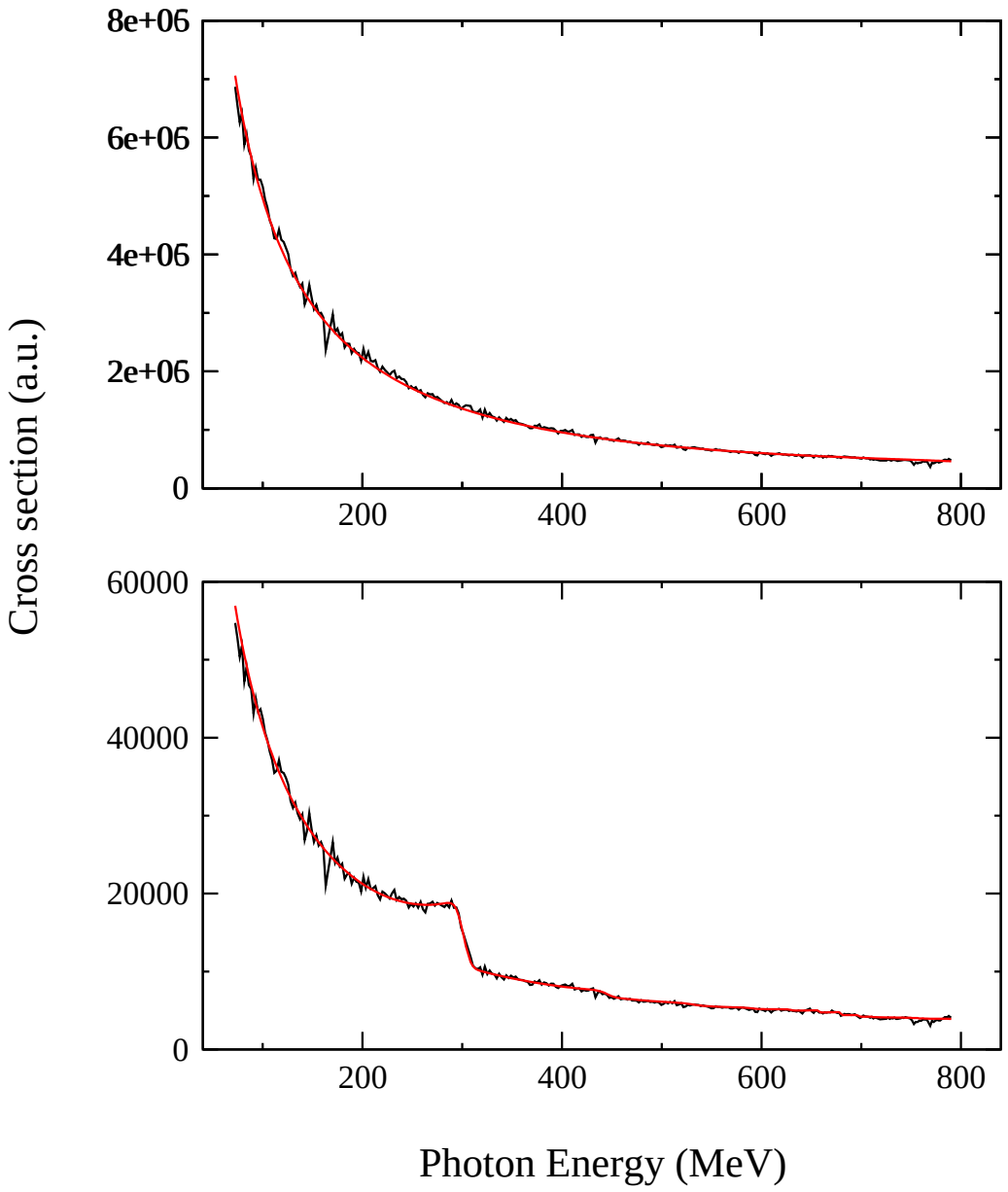

Fig. 1. Comparison of measured data (black line) and the theoretical least squares fit (red line) for the absolute bremsstrahlung intensity for nickel (top) and diamond (bottom)

where m is the electron mass and E_0 the incident electron beam energy.
Since the present paper presents coherent bremsstrahlung spectra measured using the Glasgow tagged photon spectrometer at the 855 MeV electron accelerator in Mainz, we shall concentrate on coherent bremsstahlung production at 855 MeV. We shall also discuss the production at 12 GeV since this will be relevant for the planned new experiment GlueX at the Jefferson Laboratory which will use linearly polarized photons from coherent bremsstrahlung with a 12 GeV beam.
A change in the orientation of the diamond with respect to the incident elec-

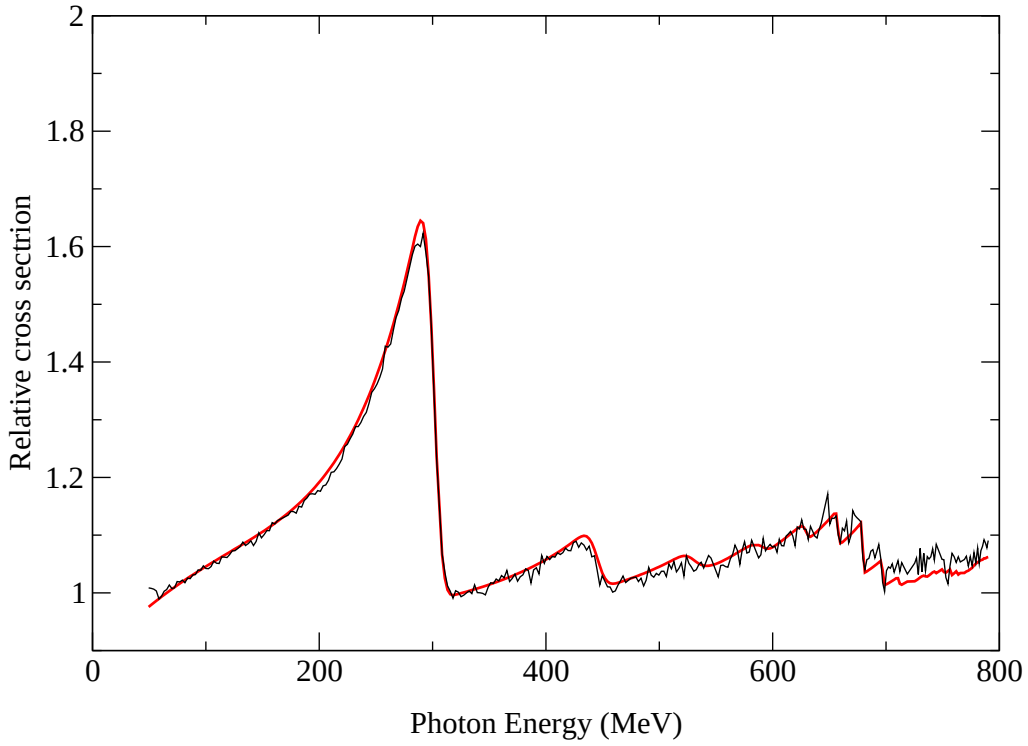

Fig. 2. Relative bremsstrahlung specrum

tron beam causes the coherent edge to shift. Figure 3 shows the magnitude of the shift for the coherent peak produced by the 220 reciprocal lattice vector for E_0 =855 MeV and E_0 =12 GeV for a range of values of $k = E_\gamma/E_0$ where E_γ is the bremsstrahlung photon energy. Indicated by the dashed lines are the shifts for E_γ=240 MeV, which is the coherent edge energy for measurements at Mainz which are discussed later in the paper, and for E_γ=8 GeV, which will be a typical energy for investigating the production of exotic hybrid mesons at GlueX (5). From figure 3 we find a change of magnitude of θ_{br} in the electron direction causes the energy of the coherent peak produced by the 220 reciprocal lattice vector to change by around $\sim 2\%$ and $\sim 0.4\%$ of E_0 for the energies E_γ = 240 MeV and 8 GeV discussed above. It follows that an electron angular distribution of this magnitude will broaden the structure of the coherent peak and reduce the maximum polarization. The values of θ_{br} for the Mainz and Jefferson Laboratory accelerators are around 600 μrad and 40 μrad respectively. Since the average divergence of the electron beam at Mainz is around 40 μrad (6) and at the Jefferson Laboratory around 12 μrad (5), the effect of beam divergence on the coherent bremsstrahlung spectra is small for both laboratories.

A reasonable approximation for the r.m.s. electron multiple scattering angle is given by:

$$\theta_{sc} = \frac{21.2}{E_0}\sqrt{t}$$

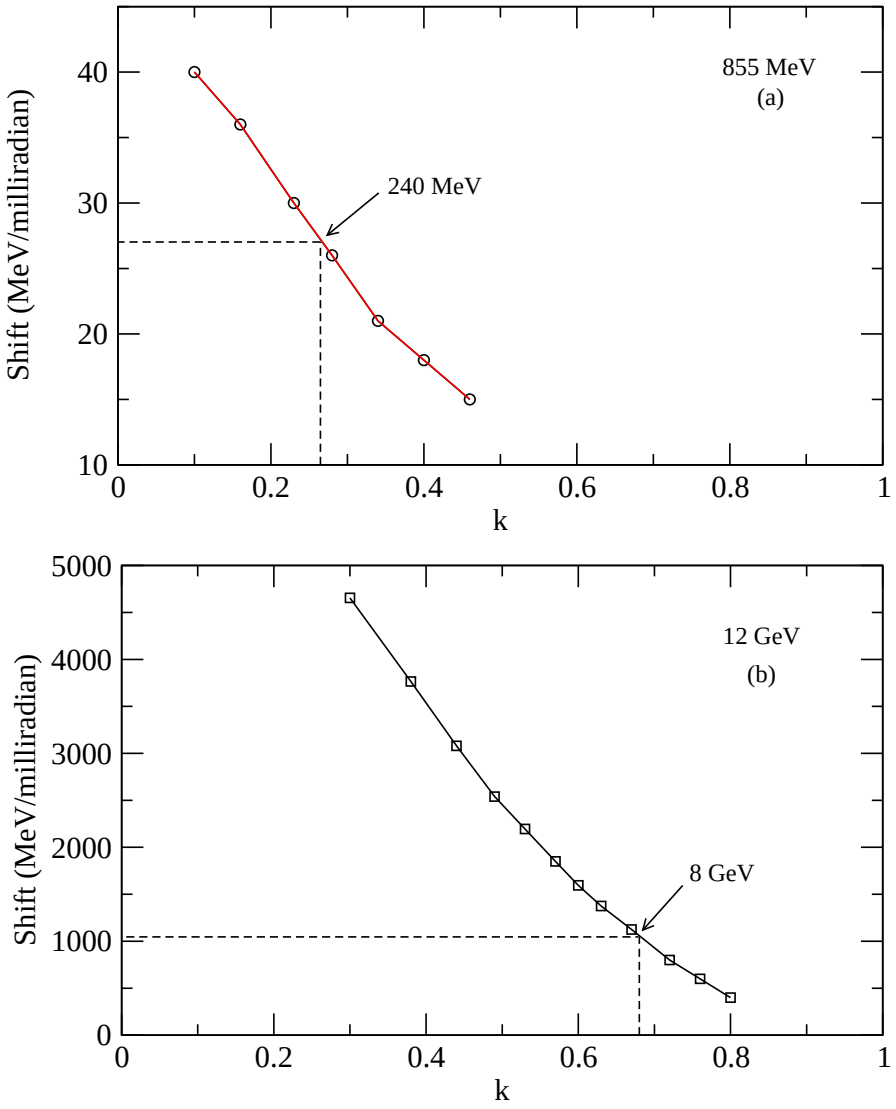

Fig. 3. Shift in position of the coherent edge from the 220 reciprocal lattice vector with respect to diamond orientation($Mev/milliradian$) for beam energies of $855MeV$ and $12GeV$ as a function of $k = \frac{E_\gamma}{E_0}$.

where E_0 is expressed in MeV and t is the radiator thickness in radiation lengths. We find, the ratio:

$$\frac{\theta_{sc}}{\theta_{br}} = \frac{21.2}{mc^2}\sqrt{t}$$

is independent of E_0, and hence a radiator of a given thickness will provide equivalent coherent bremsstrahlung spectra for different beam energies. A reasonable upper limit for which the spreading of the coherent peak and the

reduction in the polarization are small, is

$$\theta_{sc} = \frac{\theta_{br}}{2}.$$

This requires a diamond of thickness 22 μm, which is 1.45 $\times 10^{-4}$ radiation lengths.
The final point affecting the spread in the direction of the electron with respect to crystal orientation concerns the occurence of crystal defects. This is addressed by trying to obtain specimens which ideally would be diamond monocrystals. Section 2 describes the techniques used to obtain specimens with highly regular lattices.

2 Apparatus and Methods

In characterising the diamonds to determine criteria for selecting the most suitable specimens to use as radiators in coherent bremsstrahlung experiments, three techniques have been used. The first is petrographic microscopy.
The samples used for the present studies are typically wafers of thickness varying from 50 to 120 μm. They are illuminated from below using polarised light, and then viewed from above through another polaroid, crossed perpendicular to the polaroid below, such that only areas where local birefringence in the crystal caused by strain fields associated with defects can be seen.
The second and third techniques allow the defects to be studied with better resolution using X-rays. The first of these is X-ray topography, in which an image of the sample is obtained from a reflected parallel beam of X-rays. Both surface or transmission topographs can be obtained. The latter sample the volume of the specimen. Variations in the lattice parameters of the crystal caused by the presence of defects result in contrast in the image.
Although the X-rays are reflected according to Bragg's law, the reflected intensity is not a delta function when plotted against the angle the crystal makes with the X-ray beam. Rather, there is a range of angles over which reflection occurs for a given set of crystal planes, and the plot of the reflected intensity over this range of angles is known as a rocking curve (7; 8). A rocking curve measurement is sensitive to crystal quality since it can determine the mosaic spread of the crystal. According to the mosaic model (16), an imperfect crystal is believed to be composed of a large number of small mosaic blocks; within each block the distribution of the atoms is perfect, but for different blocks, the crystal planes have different orientations. Usually it is assumed the mosaic distribution is Gaussian. The mosaic spread(σ_{mosaic}) is the square root of the variance of the orientation distribution. If it is assumed the rocking curve also has a Gaussian distribution,the mosaic spread can be estimated from the

List of Diamond Specimens Investigated					
Sample	*Type*	*Thickness* (μm)	*Thickness* (*rad. lengths*)	*Plane*	*Synthetic/ Natural*
1	Ib	100	7×10^{-4}	(001)	Synthetic
2	Ia	50	3.5×10^{-4}	(001)	Synthetic
3	Ib	120	8×10^{-4}	(011)	Synthetic
4	Ib	110	7.3×10^{-4}	(001)	Synthetic
5	IIa	50	3.5×10^{-4}	(001)	Natural
6	Ib	100	7×10^{-4}	(001)	Synthetic

Table 1
A listing of the samples used in this survey.

rocking curve width; ie the $FWHM = 2.35 \times \sigma_{mosaic}$. The measurement of rocking curve widths is the third technique adopted.
Although the X-rays are scattered by atomic electrons, whereas the electons in coherent bremsstrahlung are scattered by atomic nuclei, both processes are governed by the regularity of the lattice (9). Any deviations from this regularity, made apparent by the rocking curve width exceeding its theoretical value, indicate the presence of crystal imperfections or regions of stress within the crystal. The present paper has examined if there are any identifiable changes to the coherent bremsstrahlung spectrum from a diamond having a broadened rocking curve. In particular, a series of coherent bremsstrahlung spectra from a radiation damaged diamond which exhibits very large variations in rocking curve widths across the damaged region have been examined. The spectra were obtained at the MAMI-B Mainz microtron. The electron beam was passed through each crystal sample and the energies of the residual electrons measured using the Glasgow tagged photon spectrometer (10; 11). The photon energy spectrum was obtained directly from the residual electron energy spectrum. The diamond wafers were aligned relative to the electron beam according to the technique developed by Livingston (12).
The X-ray facility used was the synchrotron radiation source at Daresbury Laboratory, England. The experimental station lies at the end of an 80 m beam line ensuring that with adequate collimation the beam is effectively parallel. A double crystal diffractometer was used to align the samples in the beam. Reflected X-rays were recorded using photographic plates, for X-ray topography, or using a NaI detector for rocking curve measurements.
Section 3 presents petrographic images, topographs and rocking curves as well as measurements of coherent bremsstrahlung spectra from a variety of diamond radiators.

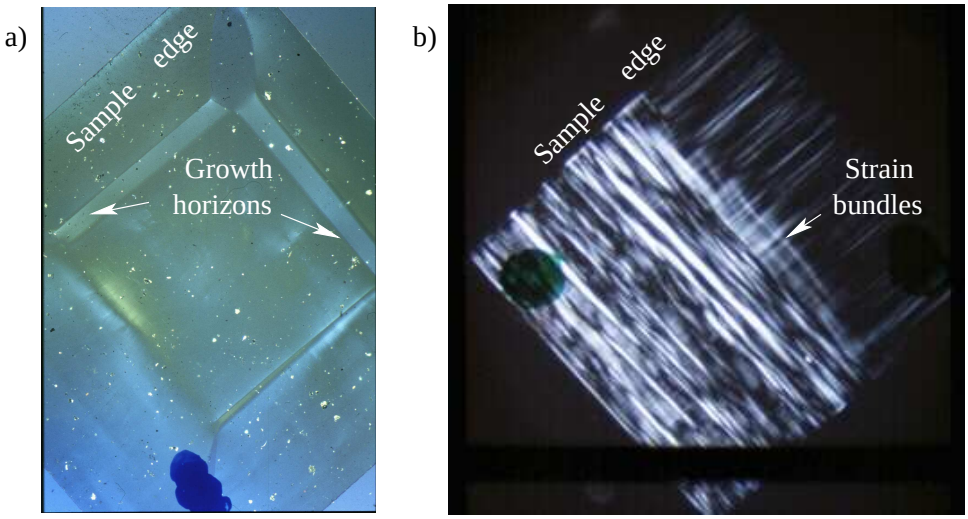

Fig. 4. Polarised light analyses of a) sample 1 and b) sample 5.

3 Results

The samples were chosen to illustrate some of the common features found in diamond wafers and also to compare different types of diamond. A list of the samples studied is shown in table 1. Figure 4 shows the polarised light analyses of samples 1 and 5 and compares a synthetic type I with a natural type II. The blue and black spots on figure 4(a) and 4(b) are identification marks. The black horizontal band at the bottom of 4(b) is an artifact of the photograph. Figure 4(a) shows an image of sample 1 taken with polarised light. It is virtually featureless, apart from some growth horizons, where strain has been induced due to differential growth rates on different families of crystal planes. There is also some dust on its surface. Figure 4(b) shows an image of sample 5 taken with polaroids crossed at 90°. It shows bundles of linear features corresponding to line defects created as the sample was undergoing metamorphosis. The presence of these bundles of linear defects, sometimes referred to as a braided strain pattern, is typical of type II samples.

Figure 5 shows the projection topographs and rocking curves of samples 1, 2 and 3, which are all type I industrial synthetic diamonds. The two vertical white lines on the topograph for sample 1 are due to the supporting wires for the sample. There is a clear similarity between the polarised light image and the topograph for sample 1. Due to its mounting, the light image is rotated by 45° with respect to the topograph but both show a central, approximately square, rather featureless region surrounded by growth horizons. Samples 1 and 2 are cut along (001) planes while sample 3 is cut along (011) planes. All three samples were chosen to have central regions in their topographs which are more or less featureless. Two rocking curves are shown for sample 1. The rocking curve shown in red corresponds to the illumination of the entire crystal by the X-ray beam. All the other rocking curves shown correspond to

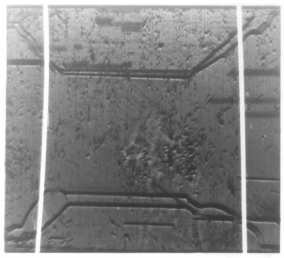

Sample 1

Projection topograph

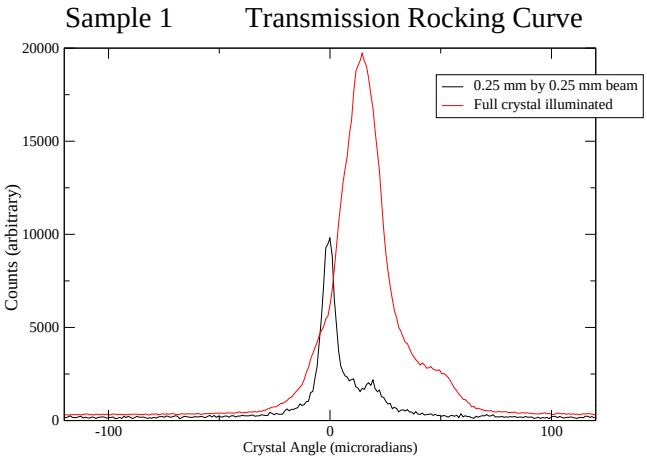

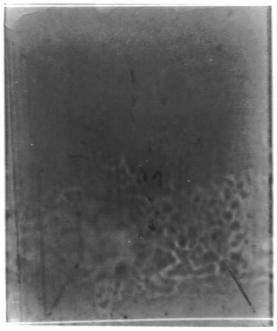

Sample 2

Projection topograph

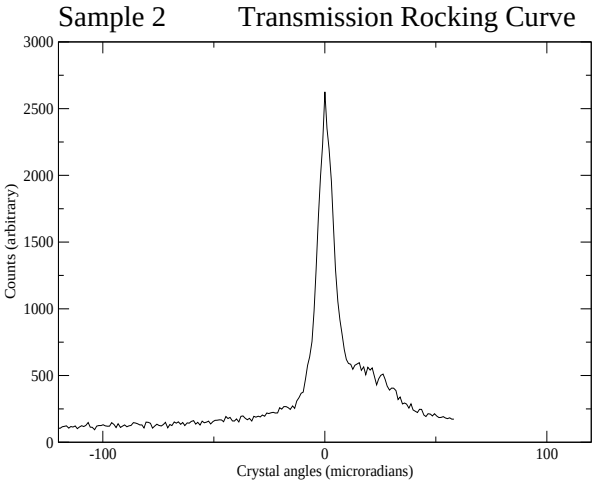

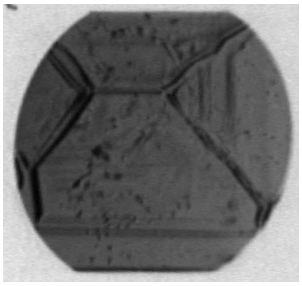

Sample 3

Projection topograph

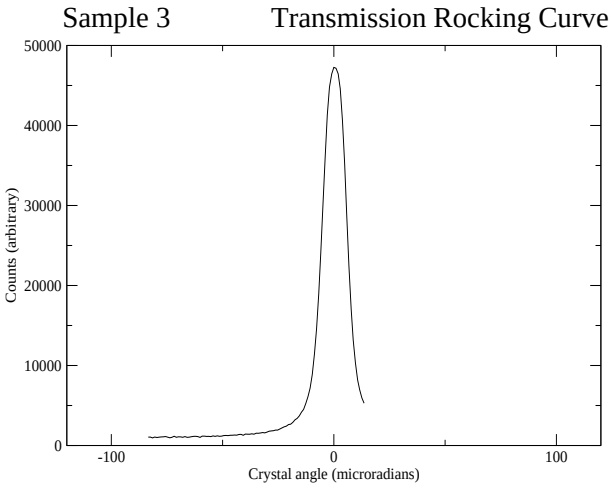

Fig. 5. Projection topographs and rocking curves of samples 1, 2 and 3.

the illumination of a central 0.25 mm square spot on the diamond. For samples 1 2, and 3 it is seen that a relatively featureless topograph correlates with a narrow rocking curve.

Figure 6 shows the topographs and rocking curves for samples 4 and 5. Sample

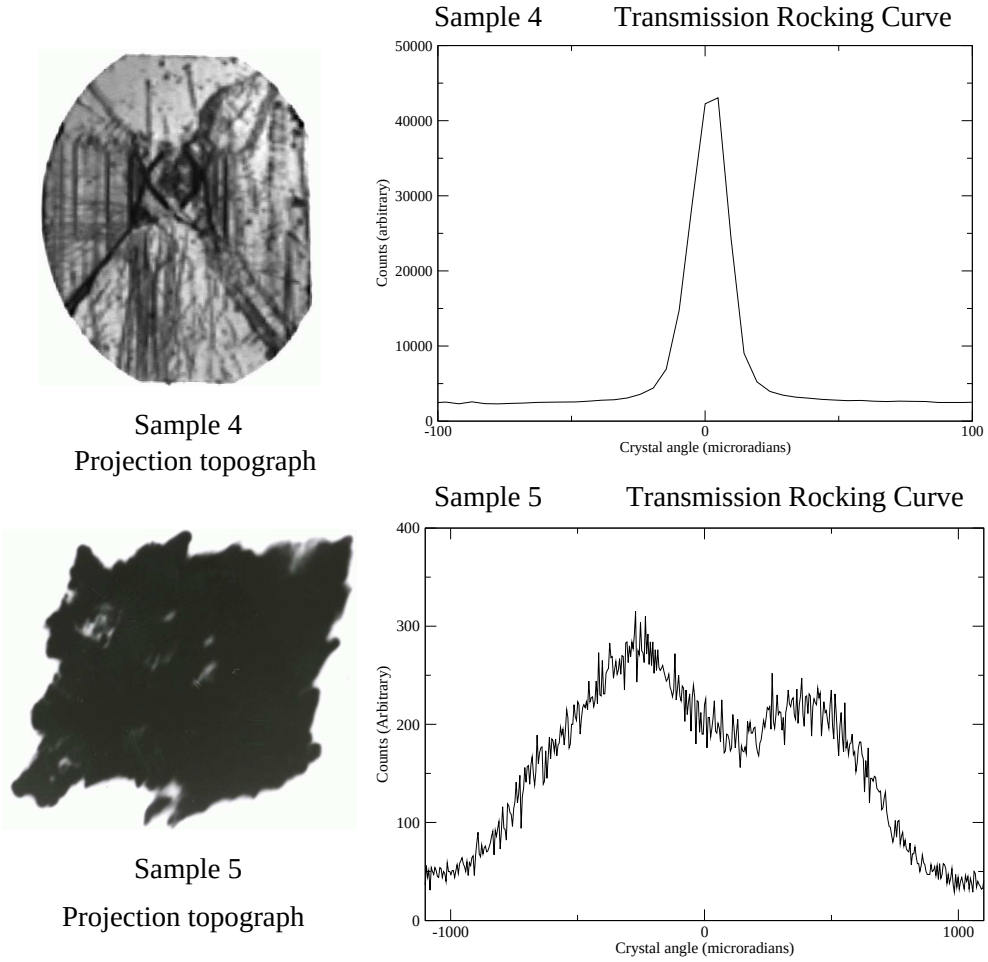

Fig. 6. Projection topographs and rocking curves of samples 4 and 5.

4 is a type I industrial synthetic whose topograph shows the imprint of the seed from which it was grown. It is seen that sample 5, a type II natural diamond, which showed considerable evidence of the strain in the polarized light analysis, has a very broad rocking curve, and its topograph is severly misshapen.

Table 2 summarises the rocking curve results from these samples. It also gives rocking curve data for a sixth sample for which coherent bremsstrahlung spectra were measured using the Glasgow tagger at Mainz. The F.W.H.M., W_{meas}, for the measured rocking curves can be compared with the theoretical F.W.H.M., W_{th}, for an ideal lattice as predicted by dynamical X-ray scattering theory. i.e.:

$$W_{th} = 2 \times (\frac{e^2}{m_e c^2}) \times \frac{\lambda^2 |F|}{\pi a^3 \sin 2\theta_B}$$

where λ is the X-ray wavelength, a is the lattice parameter for diamond, and θ_B is the Bragg scattering angle. $F = \alpha f$ where α is an integer depending on

Rocking Curves Widths							
Sample	*Type*	λ *(Å)*	*Plane*	θ_B	*Beamsize (mm×mm)*	W_{th} *(μrad)*	W_{meas} *(μrad)*
1	Ib	1	(004)	33°.9	0.25 × 0.25	5.4	6.7
2	Ia	1	(004)	33°.9	0.25 × 0.25	5.4	8.6
3	Ib	1.3	(022)	31°.1	0.15 × 0.15	11.9	12.4
4	Ib	1.3	(004)	47°.2	0.15 × 0.15	8.6	17.5
5	IIa	1	(004)	33°.9	0.25 × 0.25	5.4	$\sim$ 1200
6	Ib	1	(004)	33°.9	0.25 × 0.25	5.4	30

Table 2
A table showing the rocking curve widths of the various samples.

the crystal reflection being used and f is the mean atomic scattering factor for electrons in carbon. The rocking curves are obtained by reflections from the (004) planes for the (001) diamonds, ie. for samples 1, 2, 4, 5, and 6, and from the (022) planes for sample 3, the (011) diamond (13). This is because these reflection planes are the closest planes, with large structure factors, parallel to the face planes of the diamond. The X-ray wavelengths were chosen to make W_{th} less than 10 μrad for the (001) diamonds. For the (011) diamond W_{th} is slightly larger, having a value of $\sim$ 12 μrad.
From the information presented in figures 5 and 6 and table 2, we can make the following observations:
a) The small X-ray spot on samples 1, 2 and 3 gives sharp structure which is not much larger than the theoretical value for a perfect crystal. It is reasonable to conclude the full widths of the distributions (which are in the range from 6.7 to 12.4 μrad) give the angular ranges of the microcrystal axes in the mosaics of the samples. It is noticeable for sample 1 that this angular range increases when the whole crystal is measured as would be expected.
b) The smooth rocking curve shape of sample 4 is consistent with this picture, but it has a more uniform range of crystal axis directions.
c) Sample 5 shows a wide range of crystal axis directions, but there is no direct evidence whether this is produced by many good quality microcrystals, or, as the strain pattern seen in the polarized light picture suggests, that deformation of the lattice is a more probable explanation.
However, it should be pointed out that although rocking curve shapes provide valuable information, they do not necessarily give the complete shape of the distribution of crystal axis directions. This is a consequence of the rapid extinction of the X-ray beam in a perfect crystal - the extinction length is a few microns. As a result, if a crystal has a large fraction of its sampled volume with the same alignment, this part of the crystal does not make its full contribution to the X-ray scattering.

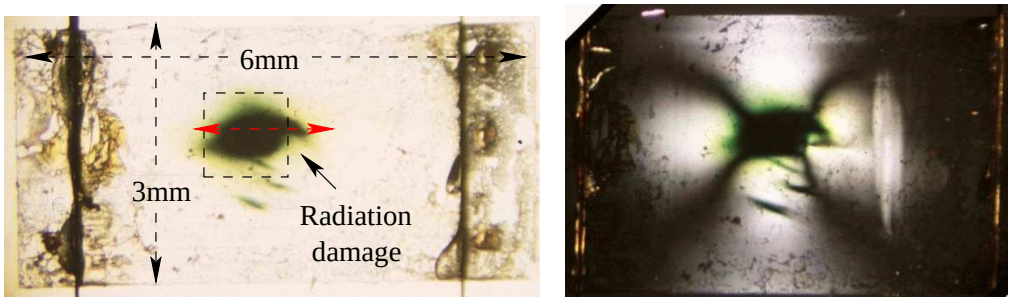

(a) (b)

Fig. 7. Petrographic microscopy of the radiation damaged diamond sample without (a) and with (b) crossed polaroids.

So far we have discussed techniques for measuring how closely the lattice structure of a diamond which has not been exposed to a high energy electron beam matches that of a perfect crystal. Using sample 6 we now describe the effect the incident electron beam has on a diamond radiator. To begin with we examine if the general shape of the coherent bremsstrahlung spectrum changes.

4 Effect of the incident electron beam.

Figure 7 shows petrographic microscopy images of sample 6, without 7(a) and with 7(b), crossed polaroids. Both images show regions of damage where the electron beam (around 10^{19} electrons in total)passed through the diamond. The dark vertical lines on the left and right of image (a) are supporting wires, and the dark areas around the wires are due to the glue holding the diamond to the wires changing colour after exposure to radiation.
The region of damage, which is outlined by the square box with dashed line edges in figure 7(a), was examined by measuring a set of rocking curves along the red line in figure 7(a) at the Daresbury SRS with an X-ray beam collimated to a square 0.25 mm^2. In addition, coherent bremsstrahlung spectra were obtained for a series of points within the damaged region at the tagged photon facility in Mainz. The electron beam was focused to a spot approximately 0.1 mm in diameter.
The rocking curves are shown in figure 8. We find that the rocking curves from the badly damaged region are much broader than those far from the damage centre. This means the damaged region has a much larger mosaic spread. From the rocking curves, we estimate the mosaic spread(σ_{mosaic}) at the damage center is about 200 μrad, and far from the damage center about 10 μrad. This indicates that away from the area which has been exposed to the electron beam, the diamond has a lattice structure which is almost perfect. The coherent bremsstrahlung spectra from the damaged region were examined by firstly looking for evidence that the damage could have changed the ratio of

coherent to incoherent bremsstrahlung between the damaged and undamaged regions of the sample.
The bremsstrahlung from a crystal has a coherent part and an incoherent part. The incoherent part also contains a crystal contribution and an electron contribution. Using a computer programme developed by Natter (14) which calculates the bremsstrahlung from both a diamond single crystal and an amorphous radiator, we find the best theoretical fit to an experimental bremsstrahlung spectrum from a diamond radiator by adding an adjustable extra incoherent component to the theoretical intensity and minimize X^2, where

$$X^2 = (I_{me} - (\alpha I_{dt} + \beta I_{nt}))^2.$$

I_{me} is the measured intensity of diamond bremsstrahlung, I_{dt} is the calculated theoretical intensity of diamond bremsstrahlung, and I_{nt} is the calculated theoretical amorphous intensity. α and β are two parameters, which are varied to minimize X^2, and hence find the best fit. The incoherent contribution I_{nt} uses the theoretical approach of Hubell (15).
The results of fitting the experimental bremsstrahlung spectra from sample 6 are summarized in table 3.

No.	1	2	3	4	5	6	7	8	9	10
x(mm)	-1.5	-1.2	-0.9	-0.6	-0.3	0	0.3	0.6	0.9	1.2
μ *(%)*	7.8	8.5	9.4	9.9	8.1	9.0	11	9.2	9.4	10

Table 3
Least squares simulation results; $\mu = \beta/\alpha$ and x is the position along the red arrowed line shown in figure 7(a). The damage centre is defined by x=0.

It is found that, after introducing the extra incoherent background, the fitted theoretical results agree well with the measured spectra. The amount of extra incoherent background is estimated by the parameter $\mu = \beta/\alpha$. The spectra were taken at different points along a line going through the radiation damaged region, where the $x = 0\ mm$ point is located at the damage center. Although, in the damaged region, the beam electrons caused many defects, as can be observed from the discoloration around the damage center and from the wide rocking curve widths, there is no significant change in the amount of extra incoherent background required between the damaged and the undamaged regions. This means the disorder caused by the radiation at the dose level and electron beam energy used, has little effect on the incoherent bremsstrahlung spectrum. It is probable that the extra incoherent background indicated in table 3 is due to limitations in the theoretical description of the bremsstrahlung spectrum from diamond.

Another factor that affects the bremsstrahlung background is the radiator temperature. The background increases with temperature, and we find the extra background in table 3 can be accounted for by assuming the radiator temperature increases to about 800 K. At present, the diamond temperature can not be measured directly during the bremsstrahlung measurements, but it is possible to estimate an upper limit for the temperature. In our experiments, the diamond radiator is glued to two vertical tungsten wires by an organic glue. Since a temperature higher than 500 K will destroy the glue, and the diamond has never separated from the wires, the radiator temperature is not very high. Theoretical predictions have also estimated that the radiator temperature does not exceed 400 K in normal conditions[14]. Hence, it is unlikely the radiator temperature will influence the incoherent part of the bremsstrahlung significantly.

Though crystal imperfections caused by the electron beam have little effect on the incoherent bremsstrahlung, we have observed some effects on the coherent part. We find that for the radiation damaged diamond (sample 6) and also a plastically deformed diamond, which is not described explicitly in the present paper, the width of the coherent edge becomes broader. The way we define the coherent edge width is illustrated in the figure 9. The two straight lines parallel to the horizontal axis go through the maximum and minimum of the coherent edge, and the third line defining the slope of the edge intersects the two horizontal lines. These two intersections define a line segment, the projection of which onto the horizontal axis defines the width of the edge. Figure 10 shows the width of the edge for different positions within the damaged region - see figure 7(a). The points are defined by x and z co-ordinates where the x axis lies along the red line shown on figure 7(a) and the z axis is at right angles to the line. It is seen that in figure 10 (b) and (c), the width changes with x, and reaches a maximum at about x=0 mm. However, in figure 10 (a) and (d), the width of the edge is almost constant. The x scans at z=0.25 mm and 0.5 mm go through the radiation damaged region, whereas the z=0 mm and 1 mm scans are outwith the damaged region.

Comparing the rocking curve measurements with the bremsstrahlung spectra for the damaged region in sample 6 we find a large mosaic spread corresponds to a broader coherent bremsstrahlung peak edge, which is consistent with the prediction of Timm (2). By referring to figure 10, it appears that there is an underlying coherent edge width of around 12.5 MeV present across the whole of the diamond, but in the damaged region this increases to around 15 MeV.

5 Discussion.

Because mosaic spread, multiple scattering and beam divergence have similar effects on the diamond coherent bremsstrahlung spectrum, we should take

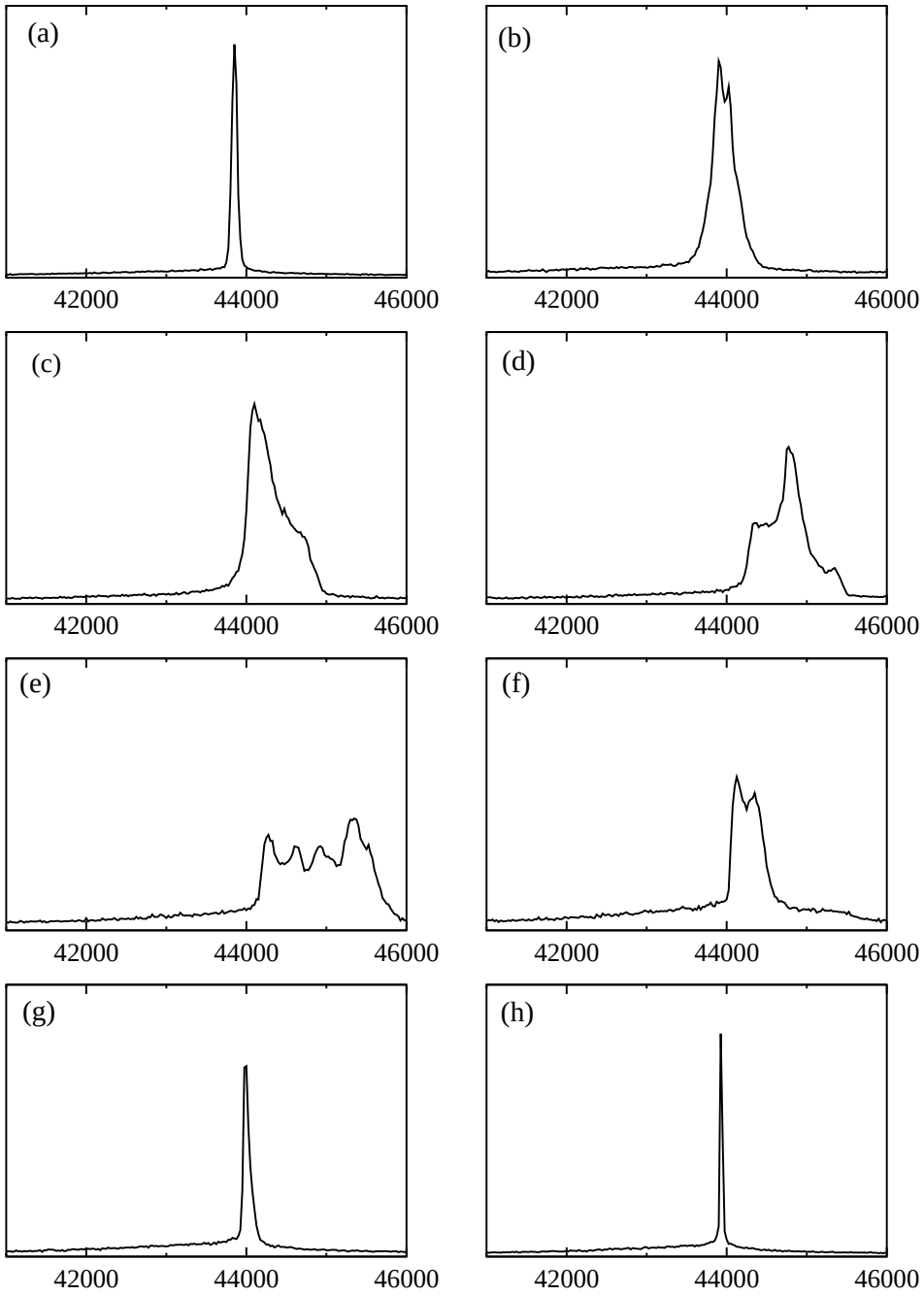

Fig. 8. Rocking curves at different positions along a line going through the radiation damaged center. For a-h, each point has a distance from the damage center of: -0.75mm, -0.50mm, -0.25mm, -0.0mm, 0.25mm, 0.50mm, 0.75mm, 1.0mm

them all into account. The total effective angular spread(σ_{total}) is given by

$$\sigma^2_{total} = \sigma^2_{mosaic} + \sigma^2_{sc} + \sigma^2_{beam}$$

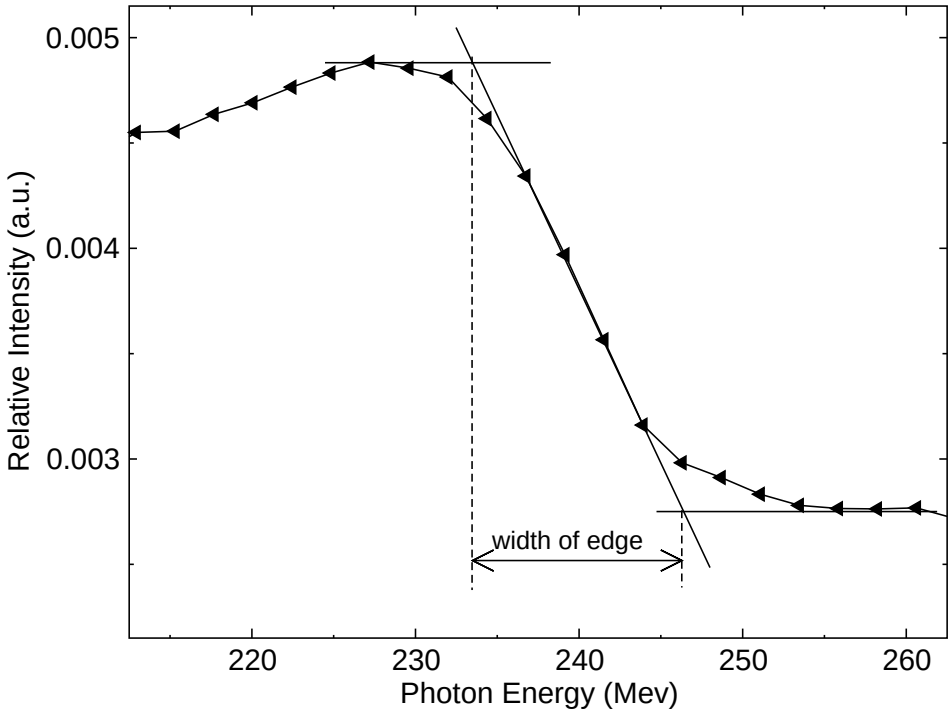

Fig. 9. Definition of the width of the coherent peak edge.

where σ_{mosaic}, σ_{sc} and σ_{beam} refer to the mosaic spread, multiple scattering and beam divergence respectively.

For the 855 MeV Mainz electron beam the bremsstrahlung characteristic angle is around 600 μrad, and for the 100 μm thick diamond (sample 6), the r.m.s. multiple scattering angle is about 660 μrad. The beam divergence was believed to be less than 100 μrad in our experiments. From the rocking curve measurements the mosaic spread is estimated to be about 200 μrad at the damage center and 10 μrad away from the damage center, hence the total effective angular spread is about 690 μrad for the damage center and 660 μrad away from the damaged region. Consequently, for the Mainz beam energy and the 100 μrad radiator used for the measurements, the overall angular spread does not change significantly even although the mosaic spread shows such a large difference between the damaged and undamaged regions. This is due to the large multiple scattering contribution from the 100 μm thick diamond. By referring back to figure 3(a), we can estimate the shifts in the coherent edge at $E_\gamma = 240\ MeV$ from angular changes of 660 μrad and 690 μrad. Values of around 18 and 19 MeV are found. These are larger than the coherent edge widths of 12.5 and 15 MeV for the damaged and undamaged regions shown in figure 10. This is to be expected since the angular spreads quoted above are for the total thickness of the diamond. The angular spread averaged throughout the thickness of the diamond would be more appropriate, but the agreement is sufficently close to provide a qualitative explanation of the results shown in figure 10.

However, the characteristic angle for a higher electron beam energy is much

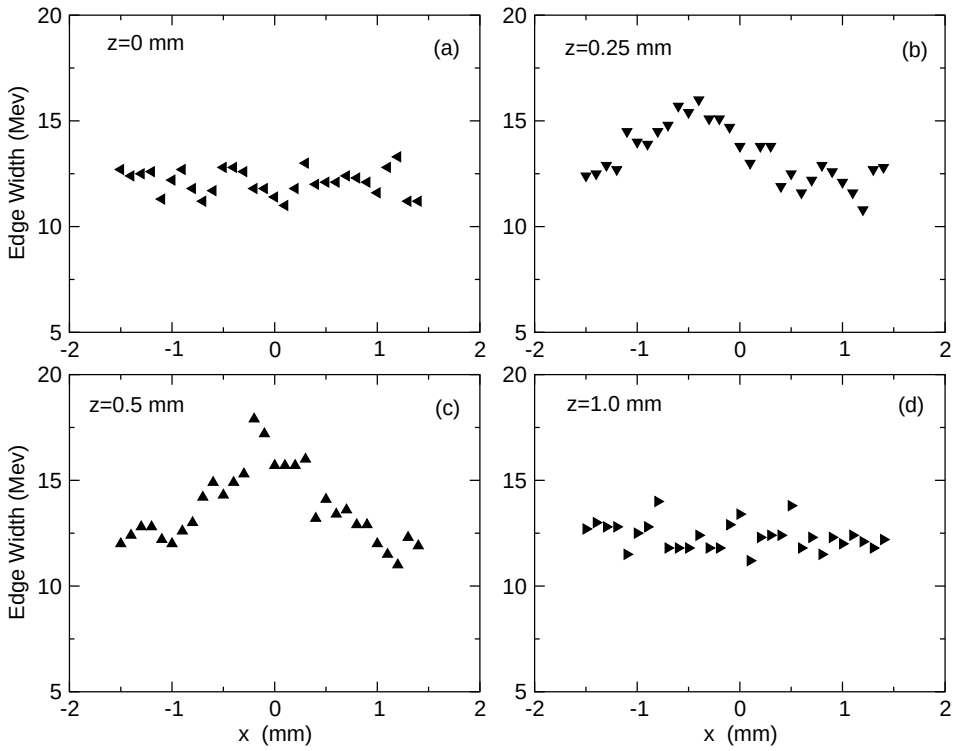

Fig. 10. The variation of the width of the coherent edge of sample 6 with x and z position. Referring to figure7 the x-axis is horizontal and the z-axis vertical, with the origin at the damage center. When z=0.25mm and 0.5mm, the x scan goes through the damaged region.

smaller, and hence much more sensitive to the beam divergence, multiple scattering, and mosaic spread. For example for 12 GeV, the characteristic angle is about 42 μrad. Hence, if we use a beam divergence of 15 μrad, which will be an average value for the GlueX project, and have a 20 μm thick diamond which has an r.m.s. multiple scattering angle of about 20 μrad, then when the mosaic spread changes from 10 μrad to 200 μrad, the overall angular spread will change from 27 μrad to 200 μrad. Referring to figure 3(b) an angular change of 200 μrad would result in a shift in the coherent edge at $E_\gamma = 8\ GeV$ of around 230 MeV The resulting smearing of the coherent bremsstrahlung peak would lead to an unacceptable decrease in the degree of linear polarisation, particularly if the photon beam is highly collimated (5). Hence, for the GlueX experiment with a 12 GeV beam, it will be essential to limit the exposure of the diamond to the beam. A total electron flux of $\sim 10^{19}$ electrons could not be tolerated.

Another important consideration for the radiation damaged diamond crystal is, that not only is there a non-uniform strain caused by the defects, but there will also be a large uniform stress caused by a slight volume expansion resulting from the large number of defects in the diamond crystal. This volume expansion has already been observed by other authors studying radiation effects (17). The petrographic microscopy of radiation damaged diamond shows

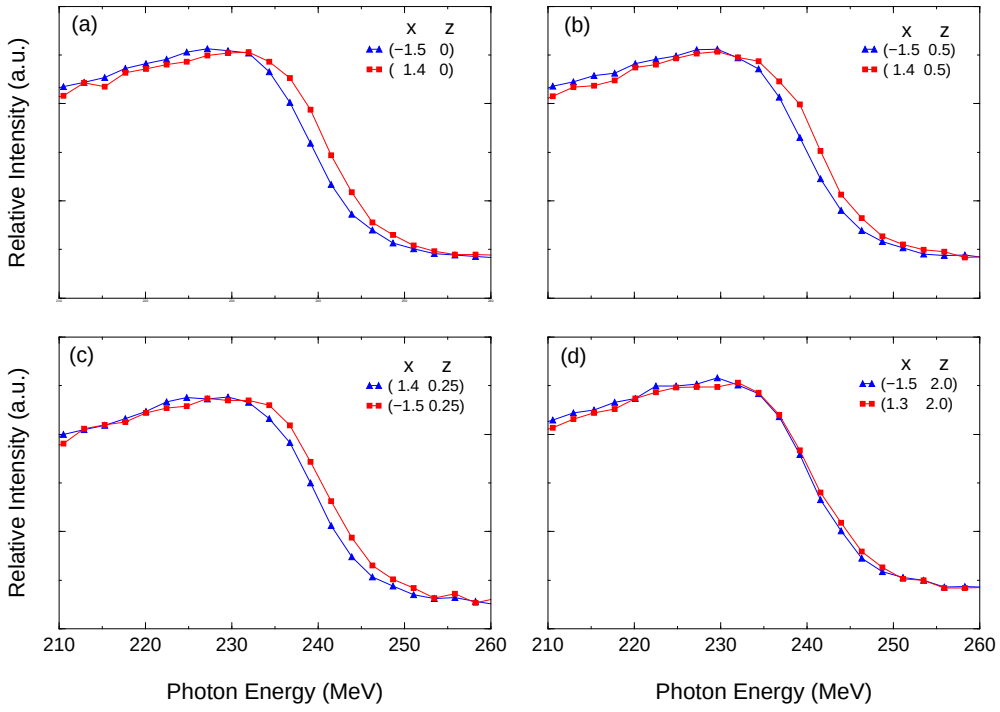

Fig. 11. Relative intensity $(I^{coh} + I^{incoh})/I^{incoh}$ of bremsstrahlung spectra for the sample 6 diamond at different positions. Referring to figure 7 the x-axis is horizontal and the z-axis vertical, with the origin at the damage centre.

a stress pattern like the stress caused by a large inclusion. It reveals a uniform strain field with 4-fold symmetry, as is shown in figure 7(b). A diamond crystal suffering from such stress will contain certain macro deformations. This means an affected diamond crystal plane will not remain flat, but will become curved, and hence the crystal orientation of different parts will be different, which will lead to a coherent peak shift. This phenomenon is readily observed experimentally for sample 6 and is illustrated in figure 11, which consists of four diagrams, each consisting of two bremsstrahlung spectra at two different points on the diamond. The coordinates of these points are shown on the top right corner of each diagram. Each pair of spectra has a common z co-ordinate, but x co-ordinates that are symmetrically placed with respect to the damage center. The spectra were taken using the same electron beam incident angle with respect to the diamond, and hence each spectrum should have the same peak position. However, from figure 11 (a), (b) and (c), a difference between the two bremsstrahlung peak positions as large as 1 to 2 MeV is seen. This is an indication that the incident angle for each point is slightly different. It is reasonable to believe that there is a different angular offset for each point indicating that the diamond is probably curved. For figure 11 (d), the peak position difference is much smaller. The two points in figure 11 (d) are farthest from the damage center, where the effect of the macro stress is expected to be smaller.

6 Conclusions.

In this paper we have considered how the angular spread of an electron beam passing through a diamond with respect to the crystal orientation is affected by the divergence of the beam , the thickness of the crystal and the presence of defects in the lattice. Irrespective of beam energy the optimum thickness of diamond is around $20\mu m$. We have demonstrated that the techniques of petrographic microscopy, x-ray topography and measuring x-ray rocking curves provide complementary information about the crystal lattice. ie: featureless petrographic and topographic images correspond to narrow rocking curves and are typical of diamonds with few lattice defects. Furthermore, it is possible to obtain diamond specimens of very high quality from synthetic industrial diamonds.
We have also discussed the effects of the incident electron beam on coherent bremsstrahlung production. The following effects have been found for sample 6, the radiation damaged diamond.

(1) The atomic disorder resulting from defects caused by the incident electron beam does not have a significant effect on the general shape of a coherent bremsstrahlung spectrum, even though the corresponding rocking curve width is significantly broadened by radiation damage.
(2) The crystal imperfections cause the coherent edge width to become broader.
(3) There is a uniform strain caused by an associated volume expansion leading to a coherent bremsstrahlung edge shift across the region of strain.

For a 12 GeV electron beam, a thin high quality diamond crystal with a small mosaic spread is essential. In particular, for a 20 micron diamond, if the mosaic spread changes by a factor of 20 from 10 to 200 μrad due to radiation damage, it is estimated the overall angular spread of the electrons will change by a factor of 7.5, from around 27 μrad to around 200 μrad. Since the resulting reduction in the degree of linear polarisation of the coherent bremsstrahlung photons would be significant, the level of damage from the electron beam should be closely monitored, ideally by rocking curve examination.

The authors acknowledge support of this work by the Engineering and Physical Sciences Research Coucil and would also like to thank the Director of the Synchrotron Radiation Source at Daresbury and the Director of the Institüt für Kernphysik at Mainz University. They also acknowledge the help received from the manager of station 7.6, Dr. David Laundy, at the SRS, Daresbury and are grateful to De Beers for supplying diamond wafers and Drukker for their expertise in polishing the diamond samples.

References

[1] D. Lohmann *et al.*, *NIM A* **343** (1994) 494.

[2] U. Timm, *Fortschritte der Physik* **17** (1969) 765.

[3] G. D. Palazzi, *Rev. Mod. Phys.* **49** (1968) 611.

[4] G. Davies, *Diamond*, Adam Hilger, (1984).

[5] The Science of Quark Confinement and Gluonic Excitations. *GlueX/Hall D Design Report*, Version 4, Jefferson Laboratary (2002).

[6] F. Rambo *et al.*, *Phys. Rev. C*, **58** (1998) 489.

[7] B. K. Tanner, D. K. Bowen, *High resolution X-ray diffractometry and topography*, Taylor and Francis, (1998).

[8] B. K. Tanner, *X-ray diffraction topography*, Pergamon, 1976.

[9] P. J. M. Clive, Ph.D thesis, Glasgow, (2002).

[10] I. Anthony *et al.*, *NIM A* **301** (1991) 301.

[11] S. J. Hall *et al.*, *NIM A* **368** (1996) 698.

[12] K. Livingston, *An Alignment Technique for Diamonds used in Coherent Bremsstrahlung Experiments*, Private communication, (2002).

[13] S. Elliott, *The Physics and Chemistry of Solids*, John Wiley and Sons, (1998).

[14] A. Natter, *A Coherent Bremsstrahlung Simulation Code*, Private communication, (2001).

[15] J. L. Hubbell, Spectrum of thin Target Bremsstrahlung bounded by a forward circular Cone, *J. Appl. Phys.* , **30** (1959) 981.

[16] C. G. Darwin, *Phil. Mag.*, **43** (1922) 800.

[17] R. Kalish, A. Reznik, et al. *Nuclear Instruments and Methods B* ,**148** (1999) 626-633.